JTTEE5 19:713–722
DOI: 10.1007/s11666-010-9478-z
1059-9630/$19.00 © ASM International

Controlling Spray Torch Fluid Dynamics—Effect on Spray Particle and Coating Characteristics

Lorenzo Vincenzi, Sho Suzuki, David Outcalt, and Joachim Heberlein

(Submitted September 15, 2009; in revised form November 24, 2009)

In order to identify means to improve plasma spray consistency, various modifications to the design of a commercial plasma torch nozzle have been investigated. The modifications consist of preparing anode inserts with grooves in the axial direction (spline insert), and introducing a fraction of the plasma gas through a ring of micro-nozzles surrounding the anode nozzle (micro-jet ring). Different designs for each modification have been investigated, and these modifications have also been paired with a modified upstream gas injector. For each of the modified designs, a wide range of characteristics have been measured for the arc, the plasma jet, the in-flight particles, and the coating. The results show that most nozzle modifications lead to higher particle temperatures and velocities. The plasma jet is significantly elongated by using some of the modified nozzles, and the cold gas entrainment somewhat reduced. Each of the nozzle modifications can be easily implemented offering an economical way to enhance process reliability.

Keywords coating evaluation, instabilities, plasma jet, plasma torch nozzle, spray particle diagnostics

1. Introduction

Plasma spraying is a coating process in which a variety of materials are injected in powder form into a high velocity, high-temperature plasma stream where they are melted and transported to a substrate to form the coating. The process has risen to prominence as more and more parts are being coated to increase their functional value, and because of the large variety of materials that can be used for coatings. The problem encountered with plasma spraying is that the process has numerous parameters that control coating quality, ranging from plasma instabilities to the atmospheric environment, and not all of these parameters can be controlled by the operator (Ref 1, 2). There have been a number of studies devoted to establishing correlations between the process parameters, principally arc current, plasma gas flow rate and composition, carrier gas flow rate and the spray particle characteristics such as average temperatures and velocities, and coating quality such as porosity and unmelt density (Ref 3-6) and general rules have been given for changing the process parameter settings to obtain reproducible coating properties. However, all of these studies used standard torch designs, and process controls were achieved by active intervention by changing process parameters.

In this paper, the process variability due to fluid dynamic effects is addressed, and torch design changes are described that would allow operation that is less sensitive to controlled or uncontrolled process variations. In particular, the fluid dynamic instabilities of the plasma jet are investigated and means to control them are presented. These instabilities are caused by the movement of the arc attachment at the anode surface, forcing a continuous change in power dissipation and plasma heating, and by the strong temperature and density gradients across the shear layer between the hot plasma jet and the cold surrounding atmospheric air (Ref 2). The arc-attachment movement results in a continuous random or quasi-periodic temperature and velocity fluctuation at the nozzle exit, which in turn leads to entrainment of cold gas from the surroundings and variation of the jet length. In addition to this upstream forcing of the plasma jet, there exist shear layer instabilities that are generated by the steep density and viscosity gradients in the shear layer between the high velocity, low density jet and the high density, cold and quiescent air environment. These instabilities generate streamwise and azimuthal vorticities, resulting in large eddy structures and again in entrainment of cold gas into the plasma jet. The consequences of this cold gas entrainment are strong variations of the temperature and velocity fields in the plasma jet on a time scale between 10^{-4} to 10^{-3} s, and non-uniform heating of the injected powder. The instabilities can be significantly reduced by using torch designs that limit the arc movement, e.g. the TRIPLEX of

Lorenzo Vincenzi, Tecnomare SpA, Via Enrico Caviglia 11, 20139 Milano, Italy; **Sho Suzuki**, Toshiba Corp Power Systems, 8, Shinsugita-Cho, Isogo-Ku, Yokohama 235-8523, Japan; **David Outcalt**, General Electric Corp., 1631 Bentley Parkway South, Minden, NV 89423; and **Joachim Heberlein**, University of Minnesota, 111 Church Str. SE, Minneapolis, MN 55455. Contact e-mails: david.outcalt@gmail.com and jvrh@me.umn.edu.

Sulzer Metco (Ref 7, 8) or the Axial Injection torch by Northwest Mettech (Ref 9), or by using vacuum plasma spraying where the plasma jet with the particles is exhausted into a low pressure chamber (Ref 10, 11); however, these solutions are coupled with increased expense.

In this paper, an improved control of the fluid dynamic instabilities is proposed by using minor modifications of the anode nozzle to modify the shear layer between the plasma jet and the surrounding atmosphere. These modifications can be coupled with a modification of the plasma gas injection ring to additionally influence the magnitude of the swirl. In combustion environments it was observed that high-velocity microjets exhausted into the shear layer were able to break up the azimuthal vorticity in the shear layer between the flame gases and the surrounding air (Ref 12, 13). In a parallel study of the fluid dynamics in a facility where the plasma jet was simulated by a jet of heated helium into a SF_6 environment yielding a similar density ratio as an argon plasma jet into a cold air environment, this break-up of the vorticity by microjets was confirmed (Ref 14, 15). In this study, the effects of microjets and some other nozzle modifications have been investigated. In particular, it was uncertain if the vorticity due to the upstream forcing, i.e. the upstream variation of pressure and velocity due to the arc-anode attachment movement, could be influenced by the nozzle modifications as drastically as they were able to influence the low-temperature low-density jets. Therefore, the effect of these modifications on plasma jet appearance and stability, on spray particle velocities, temperatures and trajectories, and on coating porosity has been investigated using suitable diagnostic methods. The next section describes the experimental apparatus and procedures, including the diagnostics used, and is followed by a section presenting the results.

2. Experiment

All experiments were performed with the SG-100 plasma spray torch (Praxair Surface Technologies, Concord, NH) with all the associated equipment, and modifications were made only to the anode nozzle exit and the front plate, and to the plasma gas injection ring. The powder used throughout this study was yttria-stabilized zirconia. Most of the results were obtained with partially stabilized 8% Y_2O_3, zirconia (AI-1075) including most of the particle in-flight properties and the coating properties, while some of the in-flight particle characteristics were obtained with fully stabilized 20% Y_2O_3 zirconia (AI-1066, Praxair Surface Technologies, Concord, NH). Two commercial anode designs were used, No. 175 and No. 358 (supersonic). The following modifications were made to the first anode design (Ref 15, 16):

(1) An insert was press-fitted into the bore of the front plate with grooves in the axial direction on its inner surface (spline insert). Different lengths of this insert were used.
(2) The exit of the nozzle bore was enlarged and an insert was soldered into the bore such that the inside of the nozzle was identical to the original (micro-jet anode). The insert contained a gas manifold channel, fed by one of the powder supply channels, and either 8 or 16 micro-channels of 0.4 mm diameter surrounding the central bore. Gas flows of up to 35 slm of argon were used through the micro-channel assembly.
(3) The front plate of the torch was modified by surrounding the central bore with a shroud of 12 micro-jet nozzles (micro-jet shroud). The flow rate through the micro-jet shroud assembly was varied between 0 and 25 slm of argon.
(4) The standard swirl injector was modified by having 12 holes with a reduced off-set from the center (reduced swirl injector). The total flow area of the 12 holes was the same as the area of the 4 holes of the standard injector.

The three different nozzle modifications are shown in Fig. 1. Several combinations of these modifications were investigated, such as the modified gas injector with the various anode nozzles, and the spline insert with the microjet shroud. The torch operating parameters were 800 A arc current, 48 slm Ar and 12 slm He as plasma gas, 3.4 slm Ar as carrier gas, and a powder feed rate of 5.8 g/min for almost all the experiments reported here, and differences from these values are noted where applicable. The substrate was grit-blasted, and then heated before each deposition run to a temperature above 300 °C, and the stand-off distance was 8 cm. The coatings were deposited on mild steel substrates, and two substrates were coated at each experimental run, and at least two experiments were performed under nominally identical conditions.

Different sets of diagnostics were used for the plasma jet and in-flight particle characterization.

(1) The plasma jet length and jet fluctuations were recorded with a ControlVision camera at 100 ns exposure time. The jet length was determined as the length of the object with pixel intensities of more than 10% of the background intensity, and averages of 40 or 50 images were taken. The fluctuations were quantified by calculating the standard deviations of the intensity fluctuations of each pixel in the CCD array. Additional data were obtained recording Schlieren images with a Kodak Ektapro high-speed video camera operating at framing rates of up to 40,500 frames per second, and a Matlab image analysis code was used to determine the jet length and shear layer thickness.
(2) The in-flight particle characteristics were investigated with the DPV 2000 (Tecnar Automation, Montreal, Canada), and the lateral distributions of particle velocities, temperatures, and particle fluxes (fraction of particles passing through a control volume at a given distance from the spray torch axis) in a plane 8 cm from the nozzle exit were determined. For each of two runs, particle properties were obtained at each of 14 radial positions as averages of 5000 particles.

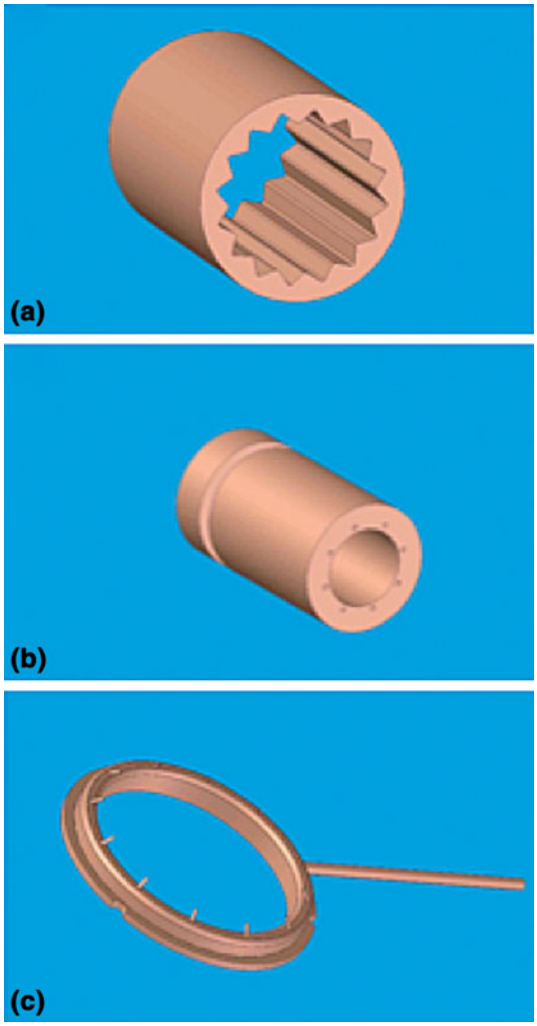

Fig. 1 Schematic of anode nozzle modifications: (a) spline insert, (b) microjet anode, and (c) microjet shroud

The lateral positions were varied from 16 mm below the torch axis (powder injection was from above) to 8 mm above the torch axis. These average velocities or temperatures obtained at each of the 14 lateral positions were weighted with the fraction of the particle flux at this radial position. Calculating average values for these 14 weighted average velocities and temperatures yielded the average velocity and temperature at a given axial location. For each radial position, the standard deviations of the particle properties were calculated from the 10,000 data points (two experiments yielding 5000 points each). The average standard deviation values were obtained by weighting the standard deviation values at each radial position with the relative particle fluxes at these positions, and then determining the averages for these weighted standard deviation values.

In addition, the plasma jet intensity fluctuations and the arc voltage fluctuations were recorded. However, the arc voltage and the total luminosity fluctuations are little

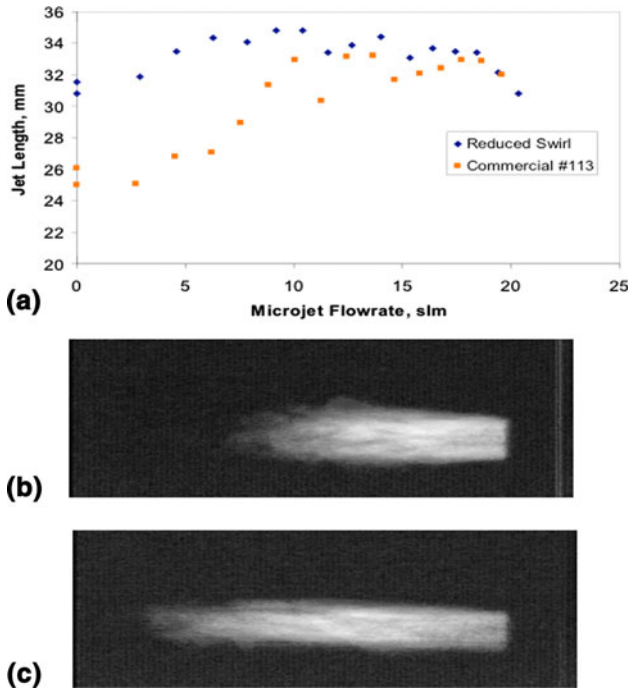

Fig. 2 (a) Average plasma jet length from 40 averaged images for different microjet flowrates using the 16 microjet anode insert, with the commercial #113 and reduced swirl gas injectors at 800 A, 48 slm Ar, 12 slm He; (b) the standard deviation of pixel intensities for 40 images with the commercial torch; and (c) with the reduced swirl gas injector at 10.5 slm Ar microjet flowrate (Ref 15)

affected by the nozzle modifications, but the modification of the gas injector does change the frequencies of the fluctuations. The frequency peaks in the voltage power spectrum appearing at 3, 5, and 8 kHz are strongly reduced with the reduced swirl injector, but a smaller peak around 1 kHz appeared (Ref 14).

The minimum thickness of the coatings was 150 μm. The coating cross-section analysis was performed on SEM images using MATLAB image analysis software. Porosity values are determined for each of the ten images, and the values for the ten images were averaged to give a value for a specific coating. At least two coatings were analyzed for each condition, and the porosity values given are the averages of all coatings obtained for a specific condition. Details of the coating analysis are presented in Sect. 3.

3. Results

Some typical measurements derived from the high-speed images for the jet lengths and jet intensity fluctuations are shown in Fig. 2 and 3. Figure 2 (Ref 15) shows the jet length variation with increasing argon flowrate through the 16 micro-jets in the micro-jet anode. The variations in jet length are shown for a regular and a reduced swirl gas injector. While the reduced swirl gas injector alone shows an increase in jet length in these

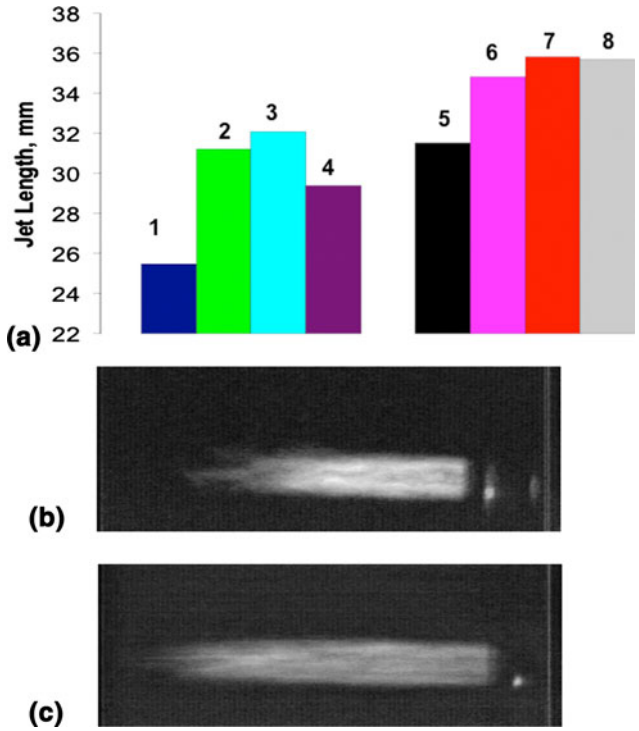

Fig. 3 (a) Plasma jet length from 50 averaged images with several spline insert lengths using the commercial #113 and reduced swirl gas injectors at 800 A, 48 slm Ar, 12 slm He, (1) standard configuration, (2) 5.75 mm spline, (3) 6.41 mm spline, (4) 7.80 mm spline, (5) reduced swirl, standard nozzle, (6) reduced swirl, 5.75 spline, (7) reduced swirl, 6.41 spline, (8) reduced swirl, 7.80 mm spline; (b) standard deviation of pixel intensities for 50 images with the commercial torch; and (c) with the reduced swirl gas injector and the 6.41 mm long splined insert (Ref 15)

experiments, this result was inconsistent with some other experiments indicating that there is at least one other parameter that needs to be considered associated with the gas injector design, possibly anode wear. The jet length reached a maximum at a micro-jet flow rate between 8 and 14 slm, and at this flow rate the jet length is increased by 40% over the standard configuration. Also shown in Fig. 2 are images of the plasma jet showing the standard deviation of pixel intensities derived from 40 images of the jet; the brightness indicates strong fluctuations. It is clear that the microjets reduce the fluctuations in the jet fringes.

Figure 3 (Ref 15) shows a similar increase in jet length when the spline insert was used. Spline inserts of different lengths were investigated, and an insert length of about 6.4 mm had the strongest effect on jet length as well as on reducing jet fluctuations. The fluctuations of the plasma jet can also be seen in Fig. 4 which displays the variation of the plasma jet tip in the lateral direction, with the negative values on the ordinate indicating the position below the torch axis. It is clearly seen that the nozzle modifications reduce the plasma jet fluctuations.

It should be pointed out that the nozzle modifications improve jet stability even though the upstream forcing due to the anode attachment movement is not influenced by the modification. That means that the large-scale vorticity generated by the upstream pressure and velocity fluctuations can be reduced by these modifications.

The effects of the nozzle modifications on in-flight particle characteristics are shown in Fig. 5 and 6 at a position 8 cm from the nozzle exit. Injection of the powder was from the positive y-direction. Figure 5 shows the radial distribution of the particle velocity averaged over 10,000 particles (two experiments with 5000 particles each) at each radial location for different nozzle configurations. Compared with the standard anode nozzle, the spline insert increases the particle velocities at almost all radial locations, the exception being the location of 6 mm above the torch axis ($y = 0$). A combination of spline insert with reduced swirl gas injector and microjet shroud yields very similar peak velocities, but a somewhat narrower particle flux distribution. The reduction of the swirl and the microjet anode reduce the particle velocities. The highest particle velocities are reached with the standard configuration of the supersonic anode. Figure 6 shows the radial distributions of the particle temperatures. All configurations tested yielded higher particle temperatures compared to the standard nozzle, except for the standard configuration with the supersonic nozzle.

The particle flux distributions as measured with the DPV 2000 at a location 8 cm from the nozzle exit are shown in Fig. 7(a) for the standard configuration and the reduced swirl injector as well as the combination of reduced swirl injector and spline insert. Figure 7(b) shows the flux distributions for the combination of reduced swirl gas injector and the microjet anode with three different flow rates through the microjets, in addition to the standard configuration and the reduced swirl configuration. The reduced swirl injector results in a narrower particle flux pattern compared to the standard injector. The other nozzle modifications have less influence on the flux pattern.

The weighted averages of particle temperatures and velocities are shown in Fig. 8 for the different configurations. This graph clearly indicates that all modifications result in higher average particle temperatures, and that spline inserts increase the velocities and temperatures while the microjets and reduced swirl injection reduce the velocities.

The standard deviations of the velocity and temperature data are believed to give some indication of process reproducibility. The standard deviations of the velocity and temperature data are given in Table 1 for selected different configurations. The use of the reduced swirl gas injector reduces the standard deviations of the particle temperatures, but the standard deviations of the velocities only in the central part of the jet because of the narrower particle flux profile. A similar effect is observed with the microjet anode or shroud. The higher peak velocities and steeper velocity gradients with the spline insert, coupled with smaller shear layer thicknesses (as determined from Schlieren images), result in larger velocity standard deviations for this configuration, but lower temperature standard deviations. One can conclude that the nozzle modifications result in higher average particle temperatures,

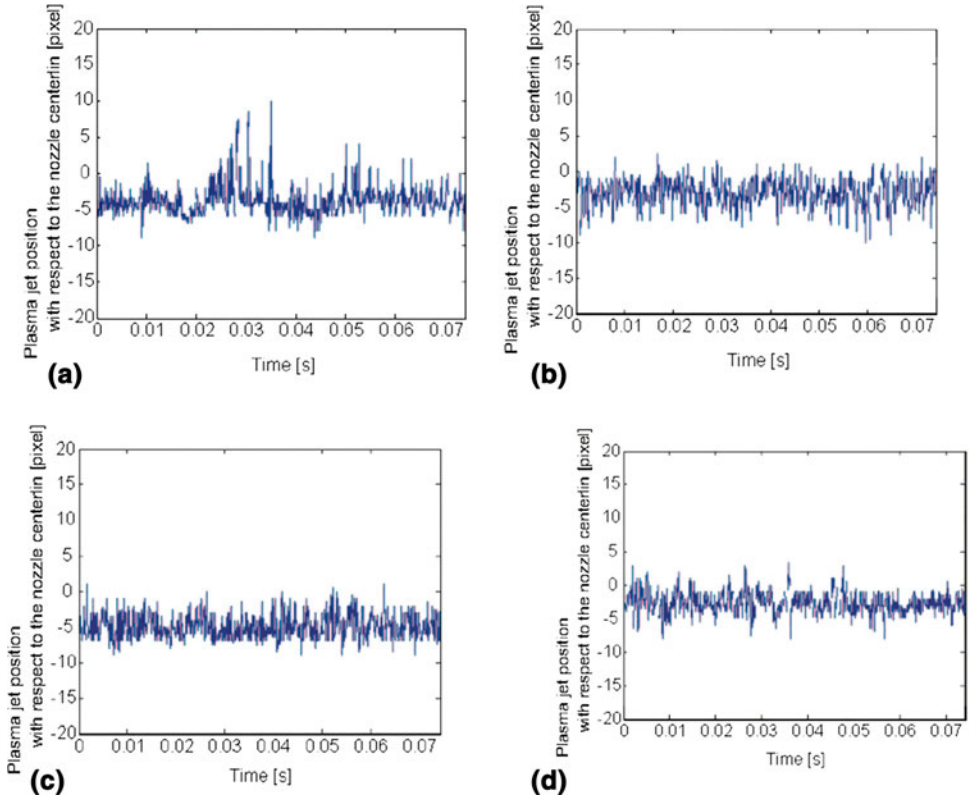

Fig. 4 Fluctuations of the plasma jet tip positioning in the lateral direction for different nozzle arrangements: (a) commercial nozzle, (b) reduced swirl gas injector, (c) long spline insert, and (d) reduced swirl gas injector and microjet anode with 9.5 slm of argon

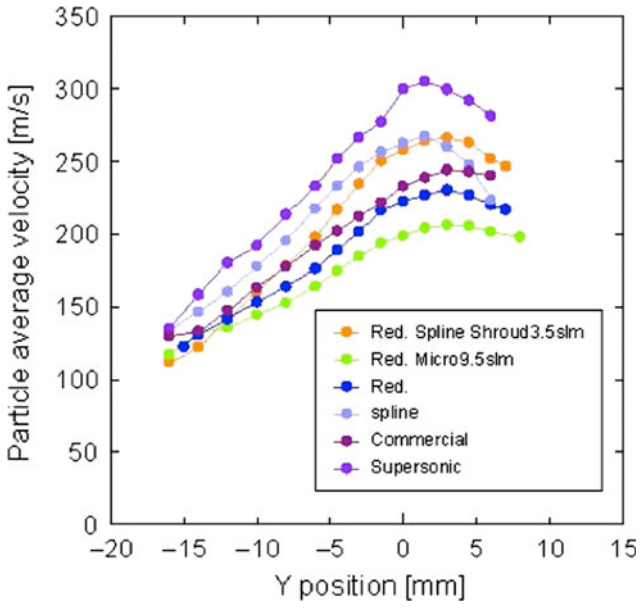

Fig. 5 Radial distribution of particle velocities for different nozzle configurations at a position 8 cm from the nozzle exit. Red. = reduced swirl injection, spline = spline insert; micro 9.5 = microjet anode with 9.5 slm argon flow and the 8 microjet anode configuration

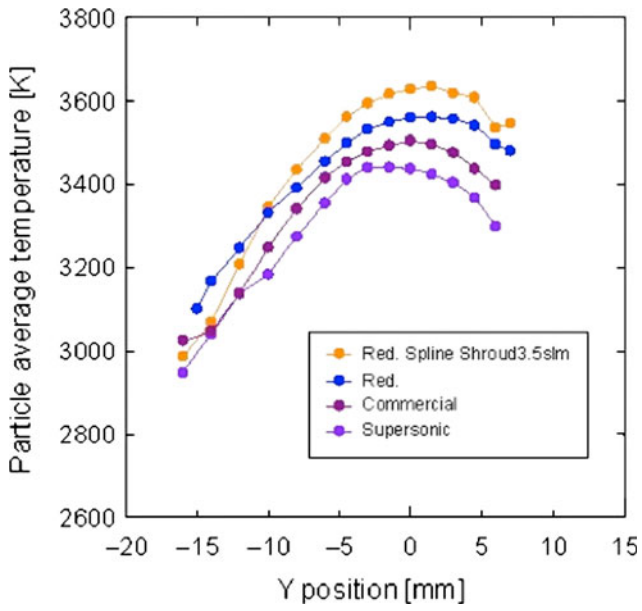

Fig. 6 Radial distributions of the particle temperatures for different nozzle configurations at a position 8 cm from the nozzle exit. Red. = reduced swirl injector, spline = spline insert; shroud 3.5 = microjet shroud with 3.5 slm of argon

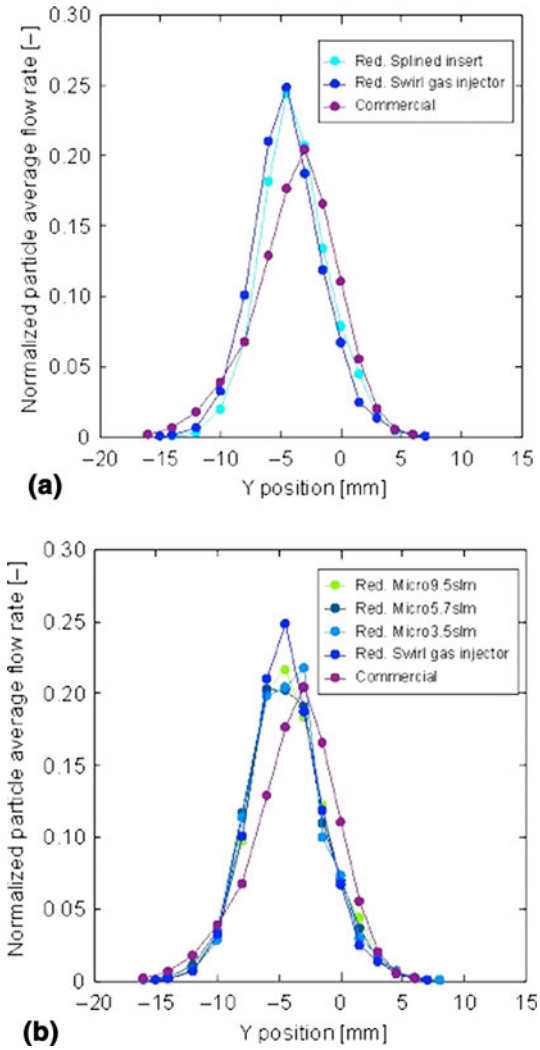

Fig. 7 (a) Normalized particle flux distributions for the standard configuration, and the standard nozzle with reduced swirl and the spline insert with the reduced swirl showing a more peaked distribution with the configurations including the reduced swirl injector; (b) normalized flux distributions for the combination of reduced swirl gas injector and microjet anode, compared with the standard configuration

lower temperature fluctuations, narrower flux profiles and steeper velocity gradients, but only the microjets with a high flow rate will reduce the velocity standard deviation.

To correlate the torch modifications and particle characteristics with the coating properties, cross sections of the coatings were analyzed with respect to total porosity, total pore porosity, small pore porosity and large pore porosity, crack porosity, and vertical and horizontal crack porosity. Figure 9 shows a sample cross section with pores and cracks indicated. SEM imaging has been chosen to acquire pictures of the coatings as it permits to obtain high-resolution images. For each substrate, 10 images at 800× magnification have been taken and 3 at 300× magnification (the latter are used only for qualitative results). The images have been analyzed using a custom made MATLAB (MathWorks Inc.) code. The process chosen to analyze the coating characteristics (SEM imaging and analysis) has proven to be quite reliable and fast, especially with respect to the most advanced, expensive and time-consuming techniques (Ref 17). In addition, the error introduced using this method is limited: as shown in Ref 18, the image analysis overestimates the porosity by 2% compared to a water immersion method. The same trend has been observed comparing image analysis with small angle neutron scattering (Ref 17): the presence of a systematical error has been observed. This systematical error has no effect on the conclusions reached in this study where relative changes in microstructure with various nozzle configurations have been investigated.

The MATLAB code basically reads the gray scale images obtained through the microscope, filters them in order to eliminate noise (using a hybrid median filter that preserves edges, thus keeping cracks sharp and visible), and converts them to black and white images. The conversion procedure requires threshold values to evaluate if the correspondent pixel in the final image will be white (gray level above threshold) or black (gray level below threshold). As the pores appear usually white while the cracks tend to be black, a double thresholding is performed, on both the original image and the inverted color image; this procedure allows all the features in the image to be clearly recognized. Threshold values of 55 and 65% have been chosen for the original and the inverted color image, respectively, and each image comprised an area of 150 × 90 μm. Cracks are recognized based on the major axis/minor axis ratio: 3.5 has been chosen as threshold value, the cracks being above the threshold. The code can then separate both pores and cracks into more groups, depending on their area.

The porosity of every single image is then calculated as the ratio of white areas and picture size, being the sum of pore porosity and crack porosity. Ten images are analyzed and average feature sizes (in pixels) and their standard deviations (as a percentage of the average value) are calculated based on all the areas in all the images taken from the same substrate. Total porosity is estimated as the average of the porosities from the ten images, and the standard deviation is computed (this value indicates the differences between the images). Crack and pore porosity are calculated in the same way as total porosity. Once the results for each substrate are obtained, an average between the two substrates of each run is made to estimate the run performance.

A regression analysis has been used to correlate the data with particle property data. The porosity values relate to average particle temperature and velocity as shown in Fig. 10 and 11 (Ref 15).

The increase in porosity with increasing velocity has also been reported by Kulkarni et al. (Ref 5). A decrease in porosity with increasing temperature is found. It should be emphasized that in this study the different particle property data have been obtained by using different nozzle configurations. The effects of particle properties on porosity are summarized in Fig. 12. The figure shows that at higher average particle velocities, the effect of an

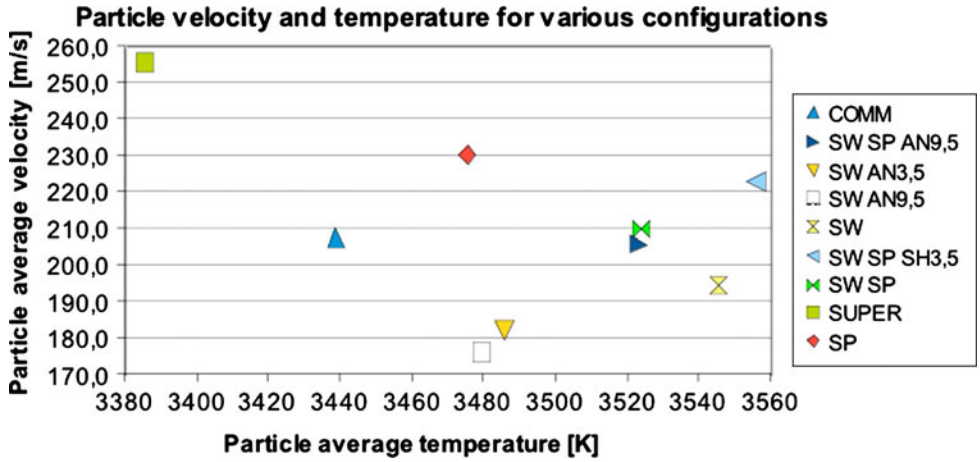

Fig. 8 Particle velocity-temperature diagram for different nozzle configurations. In all configurations, SW stands for reduced swirl gas injector. (1) COMM = standard anode and injection; (2) SP = spline insert; (3) AN 9.5 = microjet anode with 9.5 slm of argon flow; (4) AN 3.5 = microjet anode with 3.5 slm of argon flow; (5) SP, SH 9.5 = spline insert with microjet shroud with 9.5 slm of argon flow; (6) SP = spline insert; (7) SUPER = supersonic anode in standard configuration

Table 1 Average standard deviation values of temperature and velocity data weighted by particle flow rates, expressed as a percentage of the average value inside the plasma jet for different torch configurations

Configuration	Temp, SD%	Vel, SD%	Code
Stand. commercial	6.39	22.82	Com
Reduced swirl	6.04	24.28	SW
Reduced swirl microjet AN 3.5 slm	6.14	23.06	SW AN 3.5
Reduced swirl microjet AN 9.5 slm	6.11	22.23	SW AN 9.5
Reduced swirl, spline	6.18	25.62	SW SP
Reduced swirl, spline, microjet shroud 3.5	6.35	25.02	SW SP SH 3.5

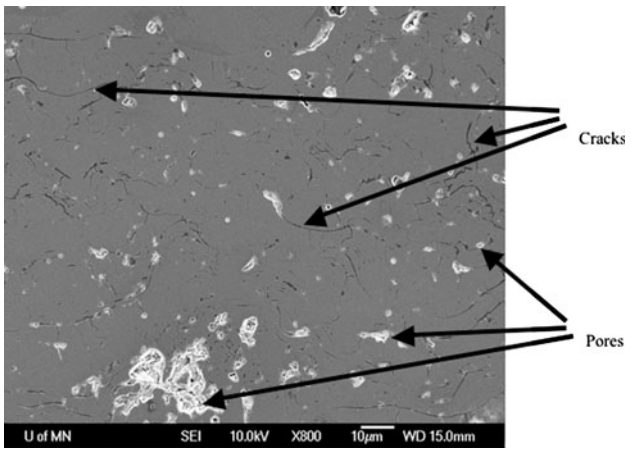

Fig. 9 Sample image of cross section of YSZ coating indicating the identification of cracks and pores

increase in temperature is more pronounced, while at higher average particle temperatures, the effect of increasing velocity is less pronounced. Table 2 gives the data for average particle characteristics and the porosity values with their standard deviations.

The following observations can be made with regard to comparison with the standard configuration:

(a) The supersonic nozzle offers approximately 25% higher velocities and about 100 °C lower temperatures, and a significantly larger fraction of unmelted particles (estimated from DPV results of particle numbers at a certain temperature), resulting in high values of porosity with low values of standard deviations, and low values of crack porosity. The size of the pores is relatively large, and numerous unmelted particles are visible.

(b) The reduced swirl injector offers lower particle average velocities, lower values for the standard deviation of the pore porosity and total porosity, associated with a narrower particle flux profile.

(c) The spline insert resulted in longer plasma jets, higher particle velocities, and some increase in temperature, resulting in high pore porosity and low crack porosity with relatively high standard deviations.

(d) The combination of micro-jet shroud and any of the other combinations could increase both particle temperature and particle velocities (at optimal flow rate).

(e) The lowest values for pore porosity and total porosity were obtained with the microjet anode, with low values of radial velocity gradients, while the highest porosity values were obtained with the supersonic anode or with the spline insert, both configurations offering high particle average velocities.

No direct correlation has been found between coating porosity and the values of the particle velocity and temperature standard deviations; however, low values for

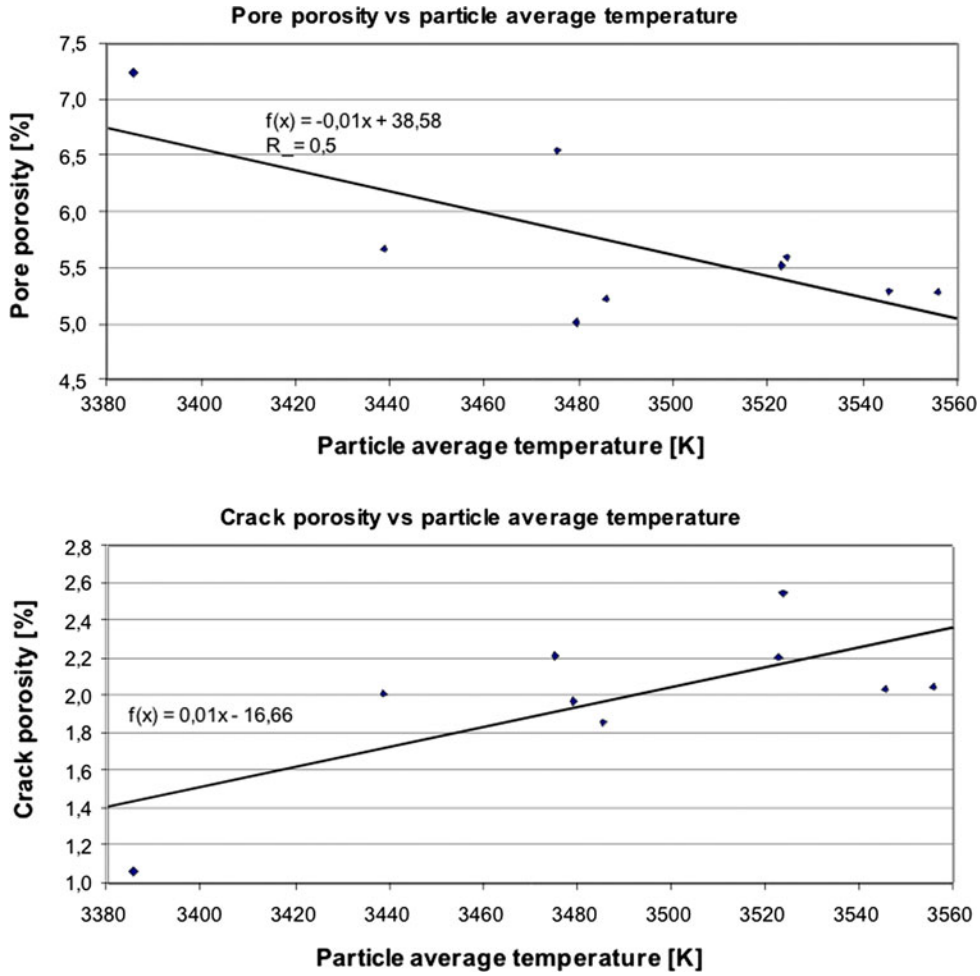

Fig. 10 Increase in crack porosity and decrease in pore porosity with increasing average particle temperature (Ref 15)

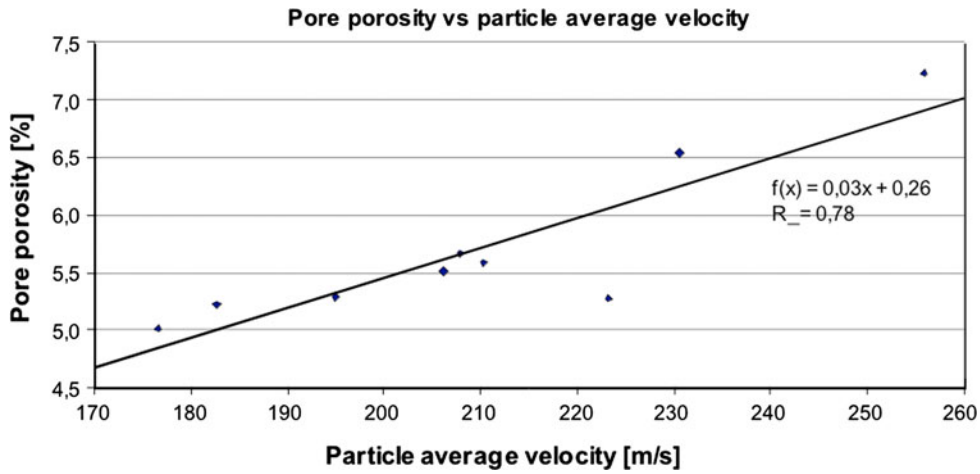

Fig. 11 Increase in total porosity with increasing average particle velocity (Ref 15)

the particle velocity standard deviations are clearly correlated with more uniform coatings, i.e. more uniformly distributed pores. Crack density values are reduced for higher particle velocities (supersonic anode, spline insert) and increased for higher particle temperatures (micro-jet anode). This behavior can be explained by increased

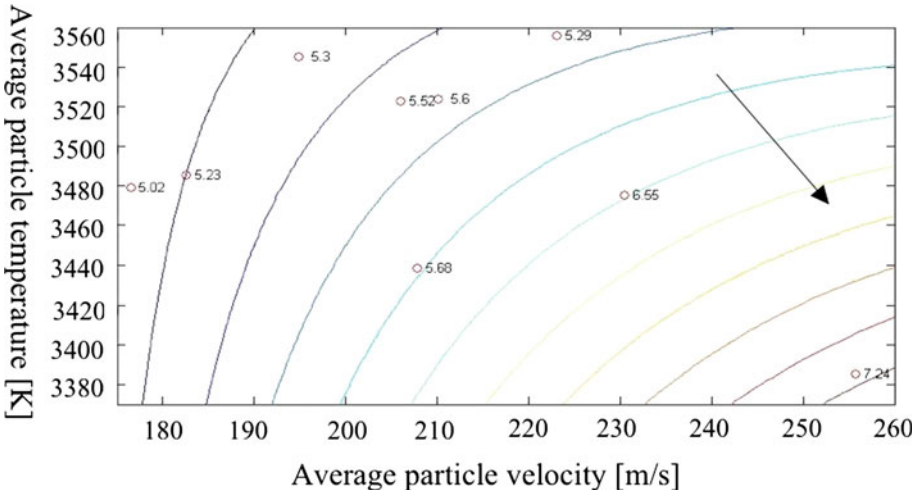

Fig. 12 Porosity iso-contours for different average particle temperatures and velocities. The arrow indicates the direction of increasing porosity

Table 2 Relations between YSZ particle average velocity (m/s), temperature (K), and velocity gradient (s^{-1}) with porosity, pore porosity, crack porosity and the standard deviations of the porosity values for different nozzle configurations

RUN	Vel	Temp	Vel grad	Porosity	SD por	Pore por	SD Ppor	Crack por	SD Cpor	RUN
COMM	207.81	3438.58	7.07	7.69	29.91	5.68	35.09	2.01	28.14	COMM
SW SP AN9,5	206.00	3522.71	9.95	7.73	17.40	5.52	20.40	2.21	36.94	SW SP AN9,5
SW AN3,5	182.56	3485.44	7.11	7.09	20.72	5.23	25.98	1.86	31.38	SW AN3,5
SW AN9,5	176.50	3479.16	5.54	6.99	20.71	5.02	28.14	1.97	28.61	SW AN9,5
SW	194.89	3545.41	8.13	7.34	16.80	5.30	20.81	2.04	27.79	SW
SW SP SH3,5	223.11	3555.75	10.45	7.42	15.10	5.29	21.60	2.05	26.65	SW SP SH3,5
SW SP	210.15	3523.79	9.60	8.15	21.33	5.60	24.96	2.55	28.94	SW SP
SUPER	255.76	3385.35	9.25	8.30	13.80	7.24	15.65	1.06	51.52	SUPER
SP	230.50	3475.23	9.17	8.76	26.25	6.55	29.93	2.21	40.71	SP
SP AN3,5				6.55	23.42	4.94	26.42	1.61	32.64	SP AN3,5

Comm = standard 175 nozzle, SW-SP-AN9.5 = reduced swirl, spline insert with microjet anode using 9.5 slm of argon; SW-AN3.5 = reduced swirl, microjet anode with 3.5 slm of argon flow; SW-AN9.5 = reduced swirl with microjet anode and 9.5 slm of argon flow, SW = reduced swirl with standard anode; SW-SP-SH3.5 = reduced swirl, spline insert and microjet shroud with 3.5 slm of argon; SW-SP reduced swirl with spline insert; SUPER = supersonic anode #358; SP = spline insert, SP-AN3.5 = spline insert with microjet anode and 3.5 slm of argon

stresses in the splats when they start solidification from a higher initial temperature (Ref 19).

One additional observation on the advantage of using a spline insert should be mentioned. The coating obtained with the spline insert was less affected by uncontrolled variations of the arc current or voltage, e.g. as generated by a misaligned cathode or a strong restrike behavior of the arc anode attachment. This observation indicates that fluid flow control in the jet can mitigate arc instabilities inside the torch.

4. Conclusions

Correlations have been derived between nozzle configurations, plasma jet appearance, particle velocity and temperature distributions, and coating characteristics. Spline inserts into the anode nozzle or a micro-jet ring change particle velocity and temperature distributions; however, to take full advantage of the effects, a combination of changes must be employed. In particular, use of a reduced swirl gas injector or a micro-jet shroud will reduce the standard deviations of the particle properties and result in more uniform coatings. Consequently, such nozzle configurations may be used as passive control devices, allowing an enhancement of the reproducibility of plasma torch operation in a wide window of operating conditions, or they may be used to enhance certain coating characteristics in combination with process parameter changes. Furthermore, the nozzle modifications act on the vorticity in the plasma jet and therefore can improve torch operation even with fluctuating anode attachment or improper cathode alignment. All changes in the nozzle configurations or gas injection are easily implemented with almost any type of plasma spray torch.

The combination of process parameter changes for the different nozzle designs requires further investigations. This is particularly true for the carrier gas flow rate and the powder injection. The results presented here may guide such further investigations.

Acknowledgment

Part of this research was funded by a grant from NSF grant number CTS-0317429.

References

1. P. Fauchais, Understanding Plasma Spraying, *J. Phys. D: Appl. Phys.*, 2004, **37**, p 86-108
2. E. Pfender, W.L.T. Chen, and R. Spores, A New Look at the Thermal, Gas Dynamic Characteristics of a Plasma Jet, *Proceedings of the 3rd National Thermal Spray Conference* (Long Beach, CA), ASM International, Materials Park, OH, 1990, p 1-10
3. M. Prystay, P. Gougeon, and C. Moreau, Correlation Between Particle Temperature and Velocity and the Structure of Plasma Sprayed Zirconia Coatings, *Thermal Spray: Practical Solutions for Engineering Problems*, *Proceedings of the 9th National Thermal Spray Conference*, C.C. Berndt, Ed., 1996 (Cincinnati, OH), ASM International, Materials Park, OH, p 517-523
4. M. Friis and C. Persson, Control of Thermal Spray Processes by Means of Process Maps and Process Windows, *J. Therm. Spray Technol.*, 2003, **12**(1), p 44-52
5. A. Kulkarni, A. Vaidya, A. Goland, S. Sampath, and H. Herman, Processing Effects on Porosity-Property Correlations in Plasma Sprayed Yttria-Stabilized Zirconia Coatings, *Mater. Eng. A*, 2003, **359**, p 100-111
6. R.L. Williamson, J.R. Fincke, and C.H. Chang, A Computational Examination of the Sources of Statistical Variance in Particle Parameters During Thermal Plasma Spraying, *Plasma. Chem. Plasma Process.*, 2000, **20**, p 299-324
7. J. Zierhut, P. Haslbeck, K.D. Landes, G. Barbezat, M. Muller, and M. Schutz, Triplex—An Innovative Three-Cathode Plasma Torch, *Thermal Spray: Meeting the Challenges of the 21st Century, Proceedings of the ITSC*, Vol 2, C. Coddet, Ed., ASM International, Materials Park, 1998, p 1375-1380
8. G. Barbezat and K. Landes, Plasma Technology TRIPLEX for the Deposition of Ceramic Coatings in the Industry, *Thermal Spray Surface Engineering via Applied Research, Proceedings of the 1st International Thermal Spray Conference* (Montreal, Canada), ASM International, Materials Park, OH, 2000, p 881-885
9. C. Moreau, P. Gougeon, A. Burgess, and D. Ross, Characterization of Particle Flows in an Axial Injection Plasma Torch, *Advances in Thermal Spray Science & Technology, Proceedings of the 8th National Thermal Spray Conference*, C.C. Berndt and S. Sampath, Ed. (Houston, TX), ASM International, Materials Park, OH, 1995, p 141-147
10. E. Muehlberger, Industrial Plasma Processing Technology, *1st Plasma-Technik Symposium* (Lucerne, Switzerland), Plasma-Technik AG, Wohlen, Switzerland, 1988, p 105-118
11. A. Refke, G. Barbezat, J.L. Dorier, M. Gindrat, and C. Hollenstein, Characterization of LPPS Processes Under Various Spray Conditions for Potential Applications, *Thermal Spray 2003 Advances in Science and Applying the Technology, Proceedings of the International Thermal Spray Conference*, B. Marple and C. Moreau, Ed., ASM International, Materials Park, OH, 2003, p 581-588
12. V.H. Arakeri, A. Krothapalli, V. Siddavaram, M.B. Akislar, and L.M. Lourenco, On the Use of Microjets to Suppress Turbulence in a Mach 0.9 Axisymmetric Jet, *J. Fluid Mech.*, 2003, **490**, p 75-98
13. C. Shih, H. Lou, F.S. Alvi, and A. Krothapalli, Microjet Control of Supersonic Impinging Jets—Control Strategy and Physical Mechanisms, *AIAA J.*, 2002, p 2002-6009
14. D. Outcalt, M. Hallberg, G. Yang, P. Strykowsky, J.V.R. Heberlein, and E. Pfender, Instabilities in Plasma Spray Jets, *International Thermal Spray Conference*, ASM International, Seattle, WA, 2006
15. D. Outcalt, S. Suzuki, L. Vincenzi, and J. Heberlein, Effect of Spray Torch Nozzle Design Modifications on Arc and Plasma Jet Characteristics and Coating Properties, *International Thermal Spray Conference* (Maastricht, Netherlands), DVS Verlag, Düsseldorf, Germany, 2008
16. D. Outcalt, ''Investigations and Control of Instabilities in a Thermal Plasma Spray Torch,'' M.S. Thesis, University of Minnesota, Minneapolis, 2007
17. S. Deshpande, A. Kulkarni, S. Sampath, and V. Prasad, Application of Image Analysis for Characterization of Porosity in Thermal Spray Coatings and Correlation with Small Angle Neutron Scattering, *Surf. Coat. Technol.*, 2004, **187**, p 6-16
18. M. Friis, P. Nylen, C. Persson, and J. Wigren, Investigation of Particle In-Flight Characteristics During Atmospheric Plasma Spraying of Yttria Stabilized ZrO_2, Part I, Experimental, *J. Therm. Spray Technol.*, 2001, **10**, p 301-310
19. S.N. Basu, G. Ye, M. Gevelber, and D. Wrobleski, Microcrack Formation in Plasma Sprayed Thermal Barrier Coatings, *Int. J. Refract. Met. Hard Mater.*, 2005, **23**, p 335-343